Supplementary material for

Combined toxicity and mechanism of cadmium and neonicotinoid insecticide to rice (*Oryza sativa* L.*)*: Reduced antioxidant defence mediated by flavonoid

Zhaoxia Fan[a,b], Na Liu[a,b*], Fei Ge[a,b], Feng Li[a,b], Wenjun Zhou[c], Juan Gao[d]

[a] Hunan Provincial University Key Laboratory for Environmental and Ecological Health, College of Environment and Resources, Xiangtan University, Xiangtan, 411105, China

[b] Science and Technology Innovation Team of Environmental Health Effect and Collaborative Treatment of Emerging Pollutant in Hunan Provincial University, Xiangtan University, Xiangtan, 411105, China

[c] State Key Laboratory of Organic Pollution Process and Control, Department of Environmental Science, Zhejiang University, Hangzhou, Zhejiang 310058, China

[d] Institute of Soil Science Chinese Academy of Sciences, Nanjing, 210008, China

* Corresponding author: Professor Na Liu,

Email: lncindliuna@xtu.edu.cn

List of content:

Texts

Text S1. Rice Cultivation and Pollutants Exposure

Rice seeds obtained from Hunan Golden Nongfeng Seed Industry Ltd. (China) were utilized for hydroponic and field experiments. Before the experiment, the seeds were sterilized with 3% H_2O_2 for 30 min, rinsed with deionized water, and then immersed in deionized water at 25 °C in darkness, with the water being changed every 24 h. After 48 h, the rice seeds were cultured in a greenhouse with Hoagland solution under controlled conditions: 25 °C, 250 μmol photons/(m^2·s), 14 h light/10 h darkness, and 70% humidity.

The registered dose (RgD) of IMI, THI, and CLO in China is 0.06 kg a.i./ha. Therefore, the NIs were applied at a concentration of 0.06 kg a.i/ha in the field experiment. Given that one rice plant, including three seedlings, is planted at 0.25 m intervals in the field, this results in a total of 48 seedlings per square meter. At the same time, 0.006 g NIs is required per square meter. Therefore, each seedling requires 0.000125 g (0.006 g/48 plants) of NIs. However, 24 rice seedlings were inserted into each 500 mL brown glass bottle in the hydroponics experiment, Thus, the treatment groups added approximately 0.01 g/L of NIs through root exposure.

Text S2. Quantitative Analysis for Cd and NIs in Rice Tissues

The collected rice leaves and grains were freeze-dried, and 0.2 g of each sample was added into a crucible. Then, 8 mL of HNO_3 was added and the samples were soaked overnight until the yellow smoke dissipated. Subsequently, 2 mL of H_2O_2 was added, and the crucible was placed on a hot plate at 200 °C for 30 min. The temperature was

then increased to 300 °C to drive off the acid. The process was considered complete when the solution in the crucible no longer exhibited gel-like properties. Subsequently, the solution was acidified with 1% nitric acid, filtered through filter paper, and then transferred into 5 mL centrifuge tubes. The Cd content in rice samples was quantified using inductively coupled plasma-mass spectrometry (ICP-MS, NexION 300×, PerkinElmer, USA). The instrument was operated at an RF power of 1500 W with a nebulizer gas flow of 0.78 L/min and an auxiliary gas flow of 1.2 L/min. The sample flush time was set to 15 s. To mitigate polyatomic interferences, the Dynamic Reaction Cell was utilized in Kinetic Energy Discrimination mode with Helium as the collision gas. For Cd quantification, Rhodium and Indium were employed as internal standards for monitoring m/z 111 and m/z 114, respectively. Method blanks (2% HNO_3) and procedural blanks were analyzed with each batch, yielding Cd signals below 0.1% of the lowest sample or undetectable. Accuracy was validated using Certified Reference Materials (GBW10010 rice and GBW10043 rice flour), with recoveries of 98.7–99.5%. Quantification relied on external calibration curves (0–10 μg/L) for ^{111}Cd ($R^2 > 0.999$). The LOD and LOQ were 0.002 mg/kg and 0.006 mg/kg, respectively. Daily instrument performance was verified using tuning solutions (N8145051) with CeO/Ce < 2.5%. Signal drift was corrected using internal standards to maintain RSD < 3%.

For the quantification of NIs content, approximately 0.1 g of the samples was combined with 5 mL of acetonitrile, swirled for 1 min, and subjected to ultrasound for 10 min. After adding 0.5 g of NaCl and 2 g of anhydrous $MgSO_4$, the mixture was manually shaken, vortexed for 1 min, and then centrifuged at 5000*g* for 5 min.

Subsequently, 1.5 mL of the supernatant was transferred to a 2 mL centrifuge tube containing 50 mg of primary–secondary amine (PSA), 150 mg of anhydrous magnesium sulphate, and 10 mg of graphitized carbon black for purification. The extract was then vortexed for 1 min and then centrifuged at 5000*g* for 3 min. The supernatant was filtered through a 0.22 μm membrane and analyzed by high-performance liquid chromatography (Agilent 1260 Infinity, USA) equipped with a Platisil ODS C18 column (250 × 4.6 mm, 5 μm) and a UV detector (G1314F). The mobile phases consisted of acetonitrile and 0.2% formic acid (50:50, *v/v*) for IMI, (30:70, *v/v*) for THI, and (25:75, *v/v*) for CLO at flow rates of 0.75, 0.9, and 0.9 mL/min, with detection at 270, 254, and 265 nm, respectively. Method blanks (reagent blanks) and procedural blanks (matrix blanks) were processed alongside each batch of samples through identical extraction and cleanup procedures, confirming no detectable residues of IMI, THI, or CLO. Matrix-spiked recovery tests conducted at three fortification levels (2, 10, and 20 mg/kg) in triplicate achieved mean recoveries of 81.64–106.15% with RSDs consistently below 10%, satisfying the acceptance criteria of NY/T 788-2018. All samples were analyzed in duplicate to assess repeatability, with replicate injection RSDs < 5% demonstrating excellent instrumental precision. Quantification was performed using matrix-matched calibration curves prepared in blank matrix extracts (0.01–10 mg/L), which showed correlation coefficients (R^2) exceeding 0.999 for all three analytes.

Text S3. Measurement for Rice Grain Quality

The protein content was determined by the Coomassie brilliant blue method. In

detail, about 0.05 g of grains at the mature stage were added to a 50 mL conical flask containing 5 mL of 0.25% (*w/v*) NaOH. The protein extract was obtained by mixing the diluted sample after standing overnight. The absorbance of 0.1 mL of protein extract mixed with 5 mL of Coomassie bright blue stain was determined at 595 nm after a reaction for 2 min. Protein concentration was calculated using a standard curve prepared with bovine serum albumin (10–100 mg/L, $R^2 = 0.9997$).

The free amino acid content was determined by the ninhydrin chromogenic method. In detail, approximately 0.1 g of grains at the mature stage were reacted with 10 mL of acetic acid and diluted to 50 mL. The reaction solution was filtered into a 100 mL bottle using filter paper, and the residue was repeatedly rinsed. After making up to a constant volume, 1 mL of the mixed filtrate was heated with 1 mL of ultra-pure water, 3 mL of ninhydrin hydrate, and 0.1 mL of ascorbic acid at 80 °C for 15 min. After cooling, the shaken reaction liquid was diluted to a final volume with 60% ethanol and the absorbance was measured at 570 nm. Free amino acids concentration was calculated using a standard curve prepared with leucine (0.1–4 mg/L, $R^2 = 0.9990$).

The starch content was determined by the anthrone colorimetric method. In detail, about 0.04 g grains at the mature stage were added to 10 mL of 0.5 mol/L NaOH, shaken, and heated in a water bath at 60 °C until completely dispersed, then removed and cooled. The starch extract was prepared from the diluted supernatant obtained after mixing and allowing it to stand. To this extract, 1 mL was mixed with 6 mL of anthrone sulfuric acid solution and soaked in boiling water for 7 min. The absorbance of the cooled reaction liquid was then determined at 640 nm. Starch concentration was calculated

using a standard curve prepared with soluble starch (10–70 mg/mL, R^2 = 0.9994).

The content of soluble sugar was determined by the phenol method. Specifically, a sample of approximately 0.1 g of grains at the mature stage was weighed and placed in a test tube. Subsequently, 5 mL of ultrapure water was added to the test tube and the mouth of the test tube was sealed using plastic films. Next, the sealed test tube was placed in a boiling water bath for 30 min of water bath extraction to fully release the soluble sugars from the grains. After the extraction was completed, the extract was transferred to a 25 mL colorimetric tube by filtration, and the test tube and residue were rinsed repeatedly using ultrapure water until the volume of liquid in the tube reached the scale mark. Next, 0.5 mL of sample liquid was accurately drawn from the colorimetric tube and transferred to another test tube. To this test tube, 1.5 mL of ultrapure water, 1 mL of 9% phenol solution, and 5 mL of concentrated sulfuric acid were added and allowed to stand at a constant temperature for 30 min for the color development reaction. Finally, the absorbance of the sample solution was measured at 485 nm. Soluble sugars concentration was calculated using a standard curve prepared with sucrose (0–25 mg/L, R^2 = 0.9994).

Text S4. Assay for Non-enzymatic Antioxidant Content and Antioxidant Enzyme Activities

The total flavonoid content was analyzed according to literature procedures. Briefly, approximately 20 mg of lyophilized powder was added to 10 mL of 70% ethanol for extraction via ultrasonication at 60 °C for 30 min. The extraction was then oscillated at 60 °C for 2 h and centrifuged at 25 °C, 12,000 rpm for 10 min. The

supernatant was collected as a flavonoid extract. Ethanol, 5.0% $NaNO_2$, 10% $Al(NO_3)_3$, and 1 mol/L NaOH solutions were added to the extraction solution successively. The absorbance (A) was measured with a spectrophotometer (UV-510, Shanghai, China) at 510 nm. Total flavonoids were quantified using a rutin standard curve (0–80 mg/L, R^2 = 0.9992) and expressed as mg rutin equivalents per gram dry weight (mg RE/g DW).

The anthocyanin content was determined by placing 0.1 g of the sample into a centrifuge tube containing 4 mL acidic methanol, followed by extraction for 25 min under agitation at 75 °C. After filtering through a membrane, the absorbance of the supernatant was measured at 530 nm and 657 nm, respectively. Finally, the anthocyanin content was calculated using the following formula (1).

$$\text{Anthocyanin content (mg/g)} = (A_{530}\text{-}0.25 \times A_{657})/0.10 \quad (1)$$

The total phenol content was determined using the Folin-Phenol method. In brief, a 50 mg sample was placed in 10 mL of distilled water and incubated at 80 °C for 30 min in a water bath. Following incubation, the sample was centrifuged at 12,000 rpm for 10 min. Subsequently, 2 mL of the supernatant was mixed with an equal volume of Folin reagent and then treated with 10% Na_2CO_3. The mixture was allowed to stand for 1 min, after which the absorbance was measured at 700 nm, with the final volume adjusted to 10 mL. Besides, the lignin content was quantified using the acetyl bromide method. Specifically, 20 mg of sample was placed in the centrifuge tube, followed by adding 2 mL of 25% (*v/v*) acetyl bromide in glacial acetic acid. The mixture was then incubated at 70 °C for 30 min. Subsequently, the sample was mixed with 4 mL of NaOH (2 mol/L) and 0.7 mL of hydroxylamine-hydrochloric acid (0.7 mol/L), and then diluted

to 10 mL with glacial acetic acid. The absorbance was measured at 280 nm. Total phenols were quantified using a catechol standard curve (0–8 mg/L, $R^2 = 0.9991$) and expressed as mg catechol equivalents per gram dry weight (mg CE/g DW).

The activities of antioxidant enzymes, including superoxide dismutase (SOD) and peroxidase (POD), and catalase (CAT) were analyzed as described previously. For SOD determination, the treatment group contained 0.3 mL of 0.75 mmol/L nitro-blue tetrazolium (NBT) solution, 0.3 mL of 0.1 mM EDTA-Na_2, 0.3 mL of 13 mmol/L methionine (MET), 0.3 mL of 0.02 mM riboflavin, and 0.1 mL of enzyme extract, while the control group added 0.1 mL deionized water to replace the enzyme extract. After 10 min of reaction under the condition of light intensity of 4000 Lux at 25 °C, the samples were immediately placed in darkness. Adjust the zero-point using the dark control group, the activity was measured by the amount of enzyme causing 50% inhibition of NBT reduction at 560 nm. Calculate according to formula (2).

$$SOD\ (U \cdot g^{-1}FW \cdot h^{-1}) = [(A_0 - A_s) \times V_t \times 60]/(A_0 \times 0.5 \times FW \times V_s \times t) \quad (2)$$

In the formula, A_0 is the absorbance of the light control group; A_s is the absorbance of the sample group; V_t is the total volume of crude enzyme solution (mL); FW is the fresh weight of rice tissue (g); V_s is the reaction volume of crude enzyme solution (mL); and t is the color development time (min).

For POD, the reaction mixture contained 1.0 mL of 0.1% guaiacol solution, 1.0 mL of 0.18% H_2O_2, and 1.0 mL enzyme extract were incubated at 25 °C for 15 min. The activity of POD was defined by the oxidation rate of guaiacol at 470 nm. Calculate according to formula (3).

$$POD\ (U \cdot g^{-1}FW \cdot h^{-1}) = [(A_0\text{-}As) \times V_t\ ]/(FW \times V_s \times t) \quad (3)$$

In the formula, A_0 is the absorbance of the control group; A_s is the absorbance of the sample group; V_t is the total volume of crude enzyme solution (mL); FW is the fresh weight of rice tissue (g); V_s is the reaction volume of crude enzyme solution (mL); and t is the color development time (min).

The activity of catalase (CAT) was measured by the decomposition rate of H_2O_2 at 240 nm. Calculate according to formula (4).

$$CAT\ (U \cdot g^{-1}FW \cdot h^{-1}) = (C \times V_t \times 60)/(0.1 \times FW \times V_s) \quad (4)$$

In the formula, C represents the slope of absorbance (min^{-1}); V_t is the total volume of crude enzyme solution (mL); FW is the fresh weight of rice tissue (g); V_s is the reaction volume of crude enzyme solution (mL).

Text S5. Capacity for Free Radical Scavenging

To assess the total antioxidant capacity of the samples, we measured the DPPH scavenging capacity, ABTs scavenging capacity, FRAP, and ·OH scavenging capacity. Specifically, a reaction mixture of 5 μL flavonoid extract and 195 μL DPPH methanol solution (0.1 mmol/L) was incubated at room temperature for 30 min. The absorbance at 517 nm was measured using an enzyme labeler (UVM 340, Biochrom, Holliston, MA, USA). The DPPH scavenging capacity was calculated according to the following formula (5).

$$DPPH\ scavenging\ capacity = [(A_{control}\text{-}A_{sample})/A_{control}] \times 100\% \quad (5)$$

ABTs scavenging ability was determined by mixing 10 μL flavonoid extract with 200 μL ABTs working liquid, followed by incubation in a 96-well plate. The absorbance

was measured at a wavelength of 734 nm after a 5 min reaction period at room temperature, protected from light. The ABTs scavenging capacity was subsequently calculated using the following formula (6).

$$\text{ABTs scavenging capacity} = [(A_{\text{control}} - A_{\text{sample}})/A_{\text{control}}] \times 100\% \quad (6)$$

Reducing power (RP) was determined by incubating flavonoid extract (25 μL) with 1% potassium ferricyanide (50 μL) at 25 °C for 60 min. Then, 10% trichloroacetic acid (25 μL) and deionized water (75 μL) were added. The absorbance at 700 nm was measured as absorbance 1 (A_1). Next, 0.1% $FeCl_3$ (25 μL) was added to this solution and the absorbance of the mixture at 700 nm was measured again, denoted as absorbance 2 (A_2). The optical density of each sample was calculated using the following formula (7). Trolox was used as the control for the standard curve and the FRAP was expressed as Trolox equivalent (mg TE/g DW) based on a standard curve (0–100 mmol/L, $R^2 = 0.9999$).

$$\text{Reducing Power } (\Delta A_{700}) = [(A_2 - A_1)_{\text{sample}} - (A_2 - A_1)_{\text{control}}] \quad (7)$$

In the formula, ΔA_{700}: Net absorbance change at 700 nm (dimensionless); A_2: Absorbance after $FeCl_3$ addition; A_1: Absorbance before $FeCl_3$ addition; Sample: Flavonoid extract (25 μL); Control: Blank containing all reagents except extract (replaced with 25 μL ultrapure water).

The ·OH scavenging capacity was determined by Fenton method. Briefly, 125 μL of flavonoid extract was added to a mixture containing 1.4 mL of 6 mmol/L H_2O_2, 0.6 mL of 20 mmol/L sodium salicylate, and 2 mL of 1.5 mmol/L $FeSO_4$ in amber centrifuge tubes to prevent photochemical interference. The reaction was maintained at

37 °C for 1 h in a constant temperature water bath. Subsequently, the absorbance (A) was measured at 562 nm. The ·OH scavenging capacity was calculated using the following formula (8).

$$\cdot OH \text{ scavenging capacity } (\%) = [A_{control} - A_{sample})/A_{control}] \times 100\% \quad (8)$$

Text S6. Flavonoid Targeting Metabolome Analysis

Flavonoid contents were detected by MetWare (http://www.metware.cn/) based on the AB Sciex QTRAP 6500 LC-MS/MS platform. Specifically, the sample was freeze-dried, ground into powder (30 Hz, 1.5 min), and stored at -80°C until needed. 20 mg of powder was weighed and extracted with 0.5 mL of 70% v/v methanol. 10 μL of internal standard solution (4000 nmol/L) was added into the extract as an internal standard (IS) for quantification. The extract was sonicated for 30 min and centrifuged at 12,000 g under 4 °C for 5 min. The supernatant was filtered through a 0.22 μm membrane. Pooled QC samples were prepared by mixing equal aliquots from all biological samples. The sample extracts were analyzed using a UPLC-ESI-MS/MS system (UPLC, ExionLCT AD, https.//sciex.com.cn/; MS, Applied Biosystems 6500 Triple Quadrupole, https: //sciex.com.cn/). The analytical conditions were as follows: UPLC column, Waters ACQUITY UPLC HSS T3 C18 (100 mm x 2.1 mm i.d., 1.8 μm); solvent system, water with 0.05% formic acid (A), acetonitrile with 0.05% formic acid (B). The gradient elution program was set as follows: 0-1 min, 10%-20% B, 1-9 min, 20%-70% B, 9-12.5 min, 70%-95% B, 12 5-13.5 min, 95% B, 13.5-13.6 min, 95%-10% B, 13.6-15 min, 10% B. The flow rate was set at 0.35 mL/min and the temperature was set at 40 °C. The injection volume was 2 μL.

To monitor instrument stability and batch variation, one QC sample was injected every 10 analytical samples throughout the run. Total ion chromatograms from QC injections were overlaid to assess system stability visually. Coefficient of variation (CV) values were calculated for each metabolite across QC samples. Using empirical cumulative distribution function analysis, over 80% of metabolites showed CV < 0.3, confirming stable data acquisition.

Linear ion trap (LIT) and triple quadrupole (QQQ) scans were acquired on a triple quadrupole-linear ion trap mass spectrometer (QTRAP), QTRAP® 6500+ LC-MS/MS System, equipped with an ESI Turbo Ion-Spray interface, operating in positive and negative ion mode and controlled by Analyst 1.6.3 software (Sciex). The ESI source operation parameters were as follows: ion source, ESI+/-; source temperature 550 °C; ion spray voltage (IS) 5500 V (Positive), 4500 V (Negative); curtain gas (CUR) was set at 35 psi. Flavonoids were analyzed using scheduled multiple reaction monitoring (MRM). Data acquisitions were performed using Analyst 1.6.3 software (Sciex). Multiquant 3.0.3 software (Sciex) was used to quantify all metabolites. Data were processed using unit variance scaling and zero-centering (Ctr). Mass spectrometer parameters including the declustering potentials (DP) and collision energies (CE) for individual MRM transitions were set with further DP and CE optimization. A specific set of MRM transitions was monitored for each period according to the metabolites eluted within this period.

Quantification was performed using external calibration curves prepared at eleven concentrations: 0.5, 1, 5, 10, 20, 50, 100, 200, 500, 1000, and 2000 nmol/L. Standard

curves were plotted with concentration ratios (external-to-internal or external standard) on the x-axis and peak area ratios on the y-axis. All calibration curves showed correlation coefficients exceeding 0.99 (range 0.99152 – 0.99996). The flavonoid content in samples was calculated using the following formula:

Flavonoid content in samples (nmol/g) = c × V / 1,000,000 / m

Where c is the sample concentration (nmol/L) obtained from the standard curve, V is the extraction volume (μL), and m is the sample mass (g).

Text S7. Real-Time Quantitative Reverse Transcription PCR Analysis

Real-time quantitative reverse transcription PCR (real-time qRT-PCR) was conducted with three biological duplicates, and each replicate was subjected to three technical replicates. The specific primers were designed utilizing NCBI (https://www.ncbi.nlm.nih.gov/tools/primer-blast/). Total RNA was extracted from rice leaves and grains by the SteadyPure RNA Extraction Kit (without Lysis Buffer) (Accurate Biotechnology, Hunan, China), and quantified. cDNA was synthesized with the Evo M-MLV RT Premix (Accurate Biotechnology, Hunan, China). Real-time qRT-PCR was performed using the SYBR Green Pro Taq HS qPCR Kit (Accurate Biotechnology, Hunan, China) with UBQ-10 serving as the internal reference gene. The thermal cycling program included initial denaturation at 95°C for 3 min, 40 cycles of amplification (95°C for 5 s, 57°C for 30 s, 72°C for 30 s), and melting curve analysis. The relative expression was calculated by the $2^{-\Delta\Delta Ct}$ method, and the mean value was taken for statistical analysis. Prior to parametric testing, data were assessed for normality (Shapiro-Wilk test) and homogeneity of variance (Levene's test). The

experiment was carried out on the Roche LightCycler 96 system (Roche Diagnostics, USA) with a PCR program in accordance. Primers were provided by SunYa Biotechnology Co., Ltd. (Hangzhou, China). To verify the specificity of each primer, negative controls (ddH_2O) and melting curve analyses were conducted.

Text S8. Proteomic analysis

The proteomics analysis was conducted by Meiji Biotechnology in Shanghai with three independent biological replicates per treatment group. The samples were suspended in protein lysis buffer (8 mol/L urea, 1% SDS) supplemented with protease inhibitors to suppress protease activity. The mixture was then processed using a high-throughput tissue grinder for three cycles, each lasting 3 min. Non-contact cryogenic sonication was then performed for 30 min. The supernatant was collected after centrifugation at 14,000*g* for 15 min under 8 °C. The protein concentration was determined using the Bicinchoninic Acid (BCA) method with a BCA Protein Assay Kit (Thermo Scientific). Protein quantification was performed according to the kit protocol. Subsequently, SDS-PAGE electrophoresis was performed. The protein sample (100 μg) was re-suspended in Triethylammonium bicarbonate buffer (TEAB; final concentration 100 mmol/L). The mixture was then reduced with Tris(2-carboxyethyl) phosphine (TCEP; final concentration 10 mmol/L) at 37 °C for 60 min, followed by alkylation with iodoacetamide (IAM; final concentration 40 mmol/L) at room temperature for 40 min in darkness. The pellet was re-suspended in 100 μL TEAB (100 mmol/L) after centrifugation at 10,000g for 20 min under 4 °C. Trypsin was added at 1:50 trypsin to-protein mass ratio and incubated at 37 °C overnight. After trypsin digestion, the

peptides were dried using a vacuum pump. The peptides were then re-solubilized in 0.1% trifluoroacetic acid (TFA), desalted using HLB (hydrophilic-lipophilic balance) columns, and dried again using a vacuum concentrator. Finally, the peptides were quantified by UV absorption using a NanoDrop One spectrophotometer (Thermo Scientific).

Based on peptide quantification results, the peptides were analyzed by an VanquishNeo coupled with an Orbitrap Astral mass spectrometer (Thermo, USA) at Majorbio Bio-Pharm Technology Co. Ltd. (Shanghai, China). Briefly, the uPAC High Throughptu column (75 μm×5.5 cm, Thermo, USA) was used with solvent A (water with 2% ACN and 0.1% formic acid) and solvent B (water with 80% ACN and 0.1% formic acid). The chromatography run time was set to 8 min. Data-independent acquisition (DIA) data were acquired using an Orbitrap Astral mass spectrometer operated in DIA mode. DIA data were acquired with the following parameters: precursor mass range 380–980 m/z, isolation window 2 m/z, 300 scan events, HCD collision energy 25%, scan range 150–2000 m/z, AGC target 5.0e4, and maximum injection time 3 ms. The 0.6-second cycle time provided 8–13 data points across average peptide peaks (5–8 sec width). The mass spectrometry scanning range was 100~1700 m/z. The DIA raw data were imported into Spectronaut software (Version 19) for database searching, using the IRGSP_1.0_protein_2024-07-12.fasta database. The parameters are as follows up : the peptide length range was set to 7~52; enzyme cutting site was trypsin/P; the maximum missed cleavage site was 2; carbamidomethylation of cysteines as fixed modification, and oxidation of methionines

and protein N-terminal acetylation as variable modifications; protein FDR ≤ 0.01, peptide FDR ≤ 0.01， peptide confidence ≥ 99%, XIC width ≤ 75 ppm. The protein quantification method was MaxLFQ. Bioinformatic analysis of proteomic data was performed with the Majorbio Cloud platform (https://cloud.majorbio.com). *P*-values and Fold change for the proteins between the two groups were calculated using R package "*t*-test". The thresholds of fold change (> 1.2 or < 0.83) and *p*-value < 0.05 were used to identify differentially expressed proteins (DEPs). Functional annotation of all identified proteins was performed using GO (http://geneontology.org/) and KEGG pathway (http://www.genome.jp/kegg/). DEPs were further used to for GO and KEGG enrichment analysis.

Text S9. Molecular Dynamics Simulation

Molecular dynamics (MD) simulations of the protein-ligand complex were performed to explore the interaction between the receptors and ligands by using GROMACS 2020.3 software. The amber99sb-ildn force field and the general Amber force field (GAFF) were used to generate the parameter and topology of proteins and ligands, respectively. Setting the size of the simulation box so that the distance between each atom of the protein and the box was greater than 1.0 nm. Filling the box with an explicit solvent-simple point charge model (SPC216 water molecules) and replacing the water molecules with Na^+ and Cl^- counterions to make the simulation system electrically neutral. The entire system was optimized by the steepest descent method, so that the unreasonable contact or atom overlap in the system was reduced. To achieve sufficient pre-equilibration of the simulation system, the NVT ensemble and the NPT

ensemble were performed for 100 ps at 300 K and 1 bar, respectively. Subsequently, the MD simulation of 100 ns was performed with periodic boundary conditions; the temperature (300 K) and pressure (1 bar) were controlled by the V-rescale and Parrinello-Rahman methods, respectively. The Newton equation of motion was calculated using the leapfrog integration with the time step of 2 fs. The long-range electrostatic interaction was calculated by the Particle Mesh-Ewald (PME) method using Fourier spacing of 0.16 nm, and the LINCS method was used to constrain all bond lengths. The visual molecular dynamics (VMD) software version 1.9.3 and PyMOL version 2.4.1 were used to display, analyze, and animate trajectories visually. The binding free energy of the compound was calculated by gmx_mmpbsa (http://jerkwin.github.io/gmxtool).

Figures

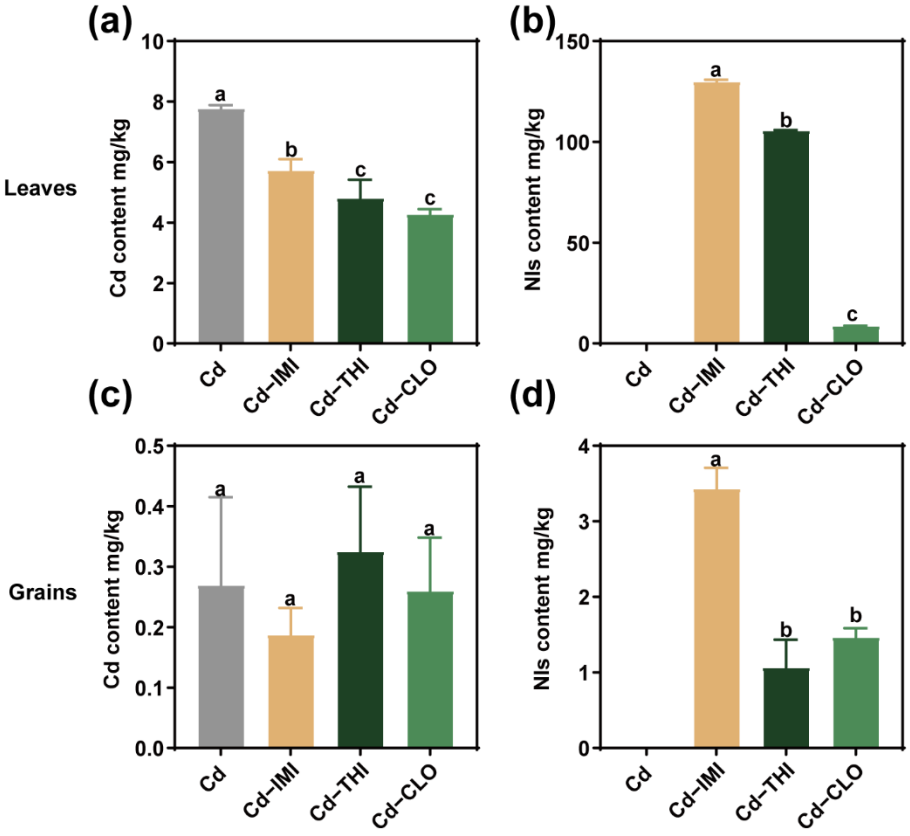

Fig. S1. Accumulation of Cd and NIs in rice tissues. Cd content changes in leaves (a) and grains (c). NIs content changes in leaves (b) and grains (d).

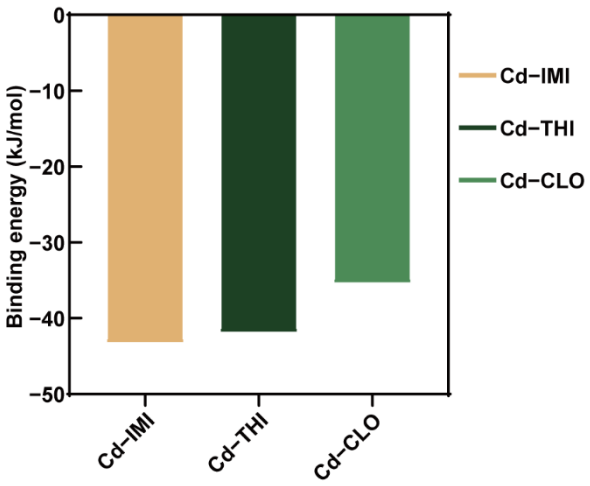

Fig. S2. Binding energies of Cd with IMI, THI, and CLO.

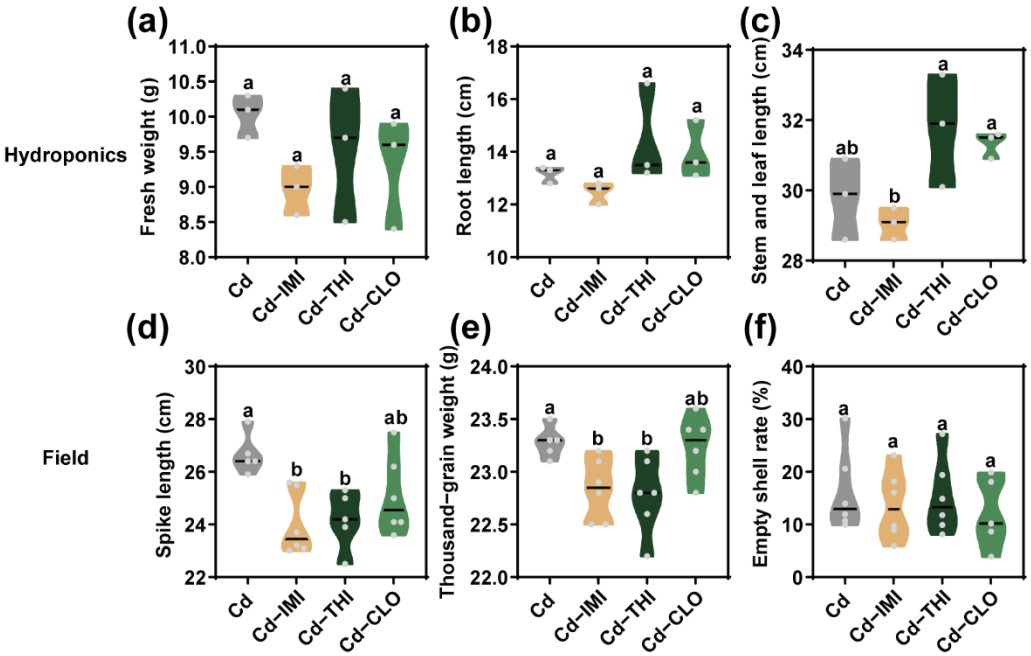

Fig. S3. Impact on rice growth and yield under the combined pollutants of Cd-NIs. Changes of fresh weight (a), root length (b), and steam and leaf length under hydroponics conditions. Changes of spike length (d), Thousand-grain weight (e), and Empty shell rate (f) under field conditions.

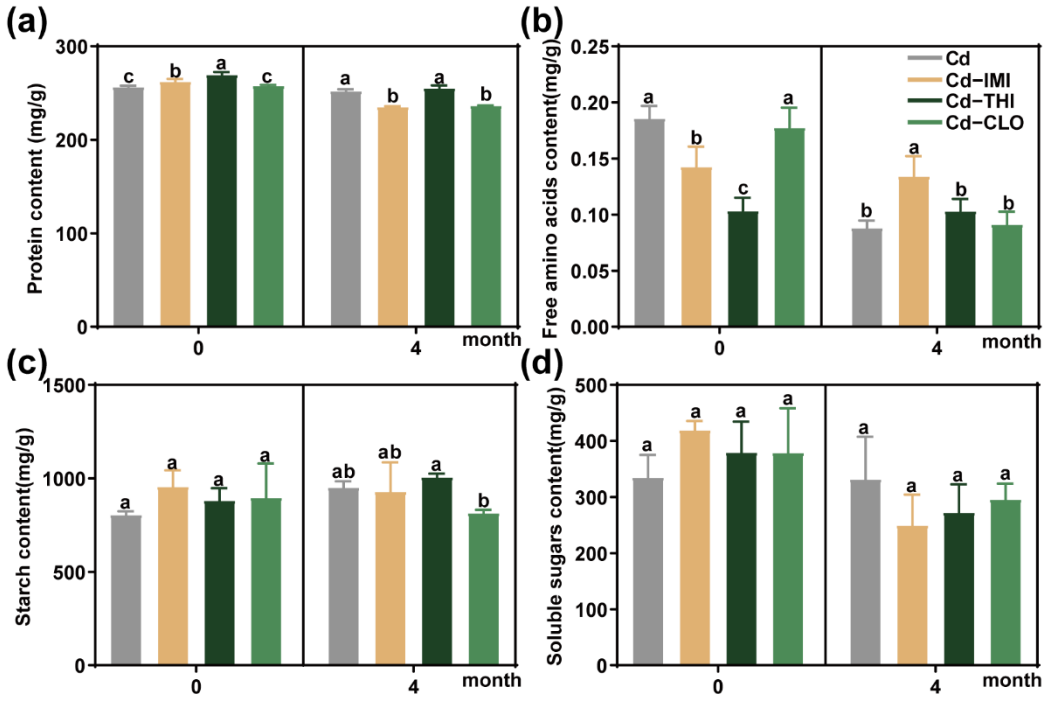

Fig. S4. Variations of nutrient contents in rice grains before and after 4 months of storage. The contents of protein (a), free amino acid (b), starch (c), and soluble sugar (d) in grains under the combined pollutants of Cd-NIs.

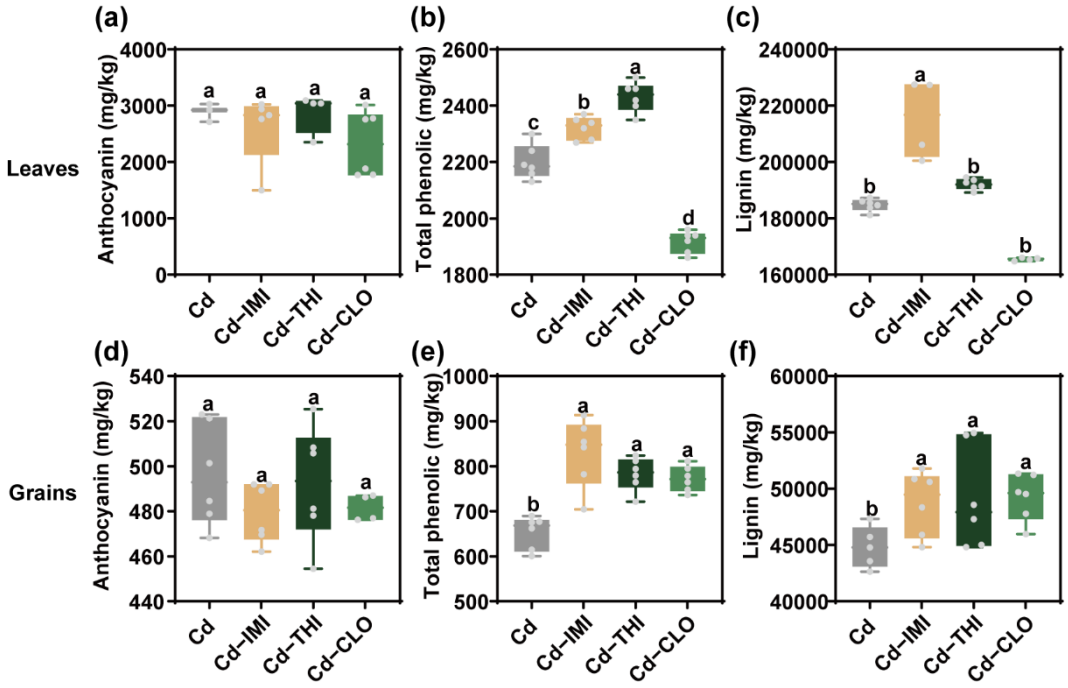

Fig. S5. Changes of non-enzymatic antioxidant content in rice tissues under the combined pollutants of Cd-NIs. Anthocyanin content changes in leaves (a) and grains (d). Total phenol content changes in leaves (b) and grains (e). Lignin content changes in leaves (c) and grains (f).

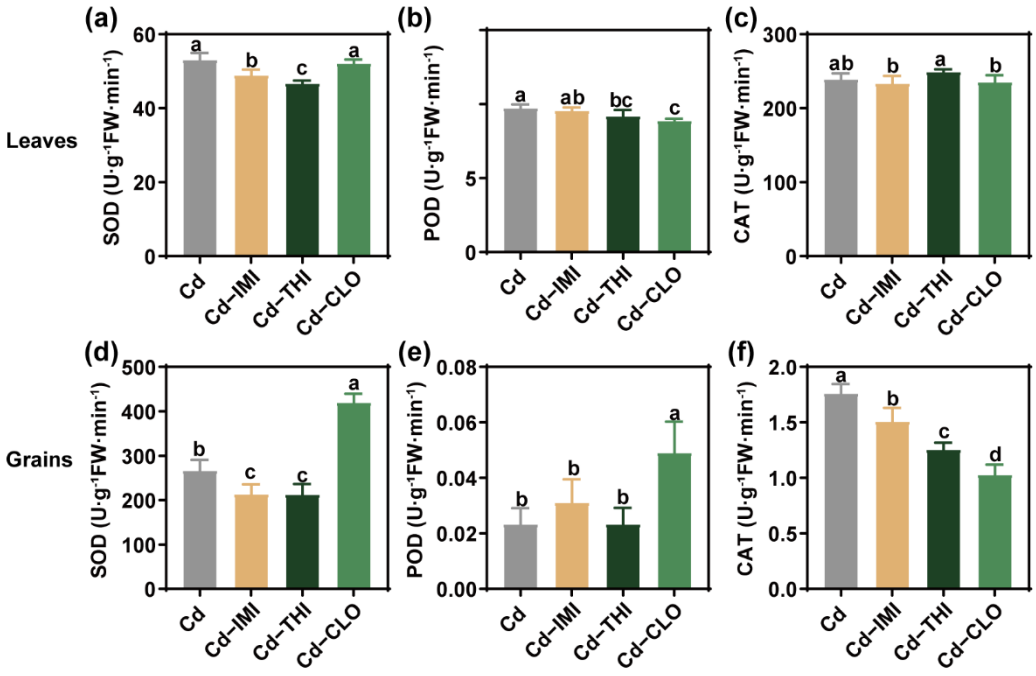

Fig. S6. Variation of antioxidant enzyme activities in rice tissues under the combined pollutants of Cd-NIs. Superoxide dismutase (SOD) activity changes in leaves (a) and grains (d). Peroxidase (POD) enzyme activity changes in leaves (b) and grains (e). Catalase (CAT) activity changes in leaves (c) and grains (f).

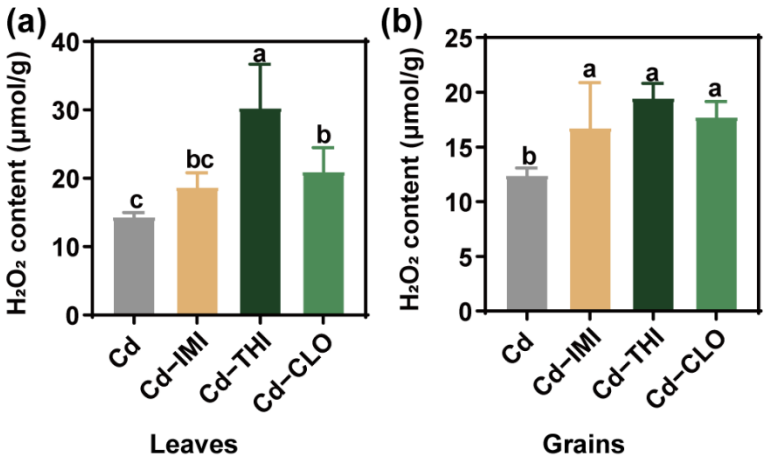

Fig. S7. Changes of hydrogen peroxide (H_2O_2) content in rice leaves (a) and grains (b) under the combined pollutants of Cd-NIs.

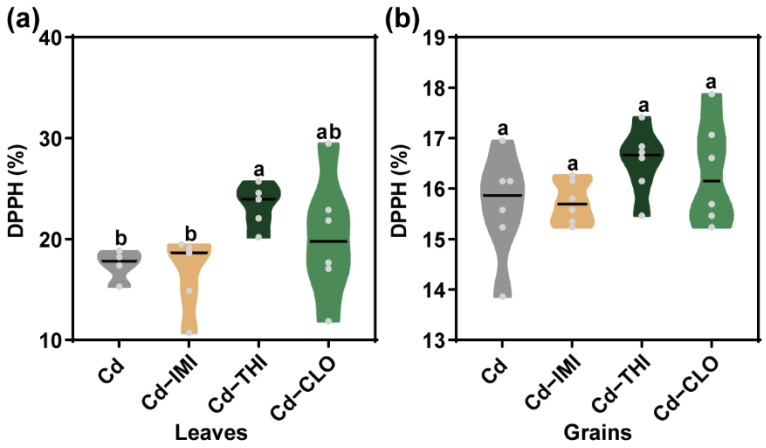

Fig. S8. Changes of 2,2-Diphenyl-1- picrylhydrazyl (DPPH) scavenging capacity in rice leaves (a) and grains (b) under the combined pollutants of Cd-NIs.

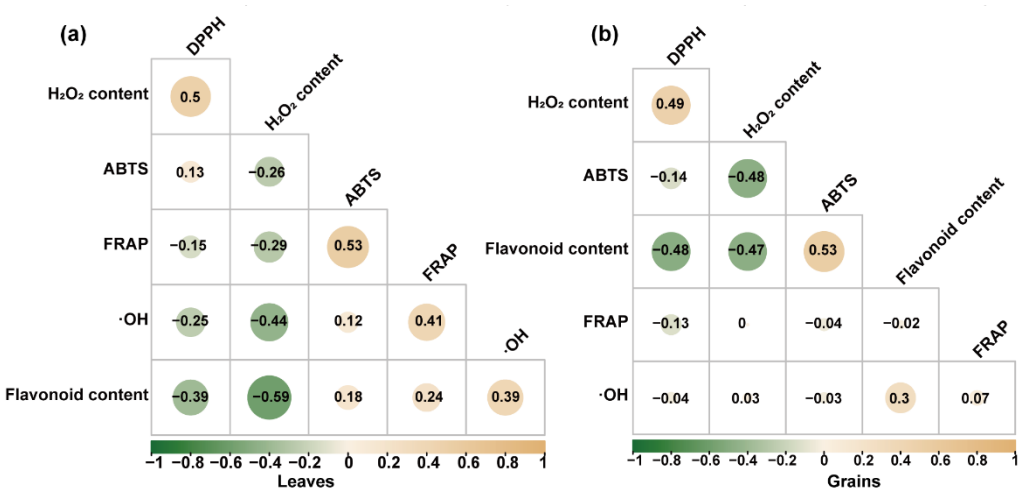

Fig. S9. Correlation analysis of flavonoid content with H_2O_2 content and free radical scavenging capacity in the leaves (i) and grains (j).

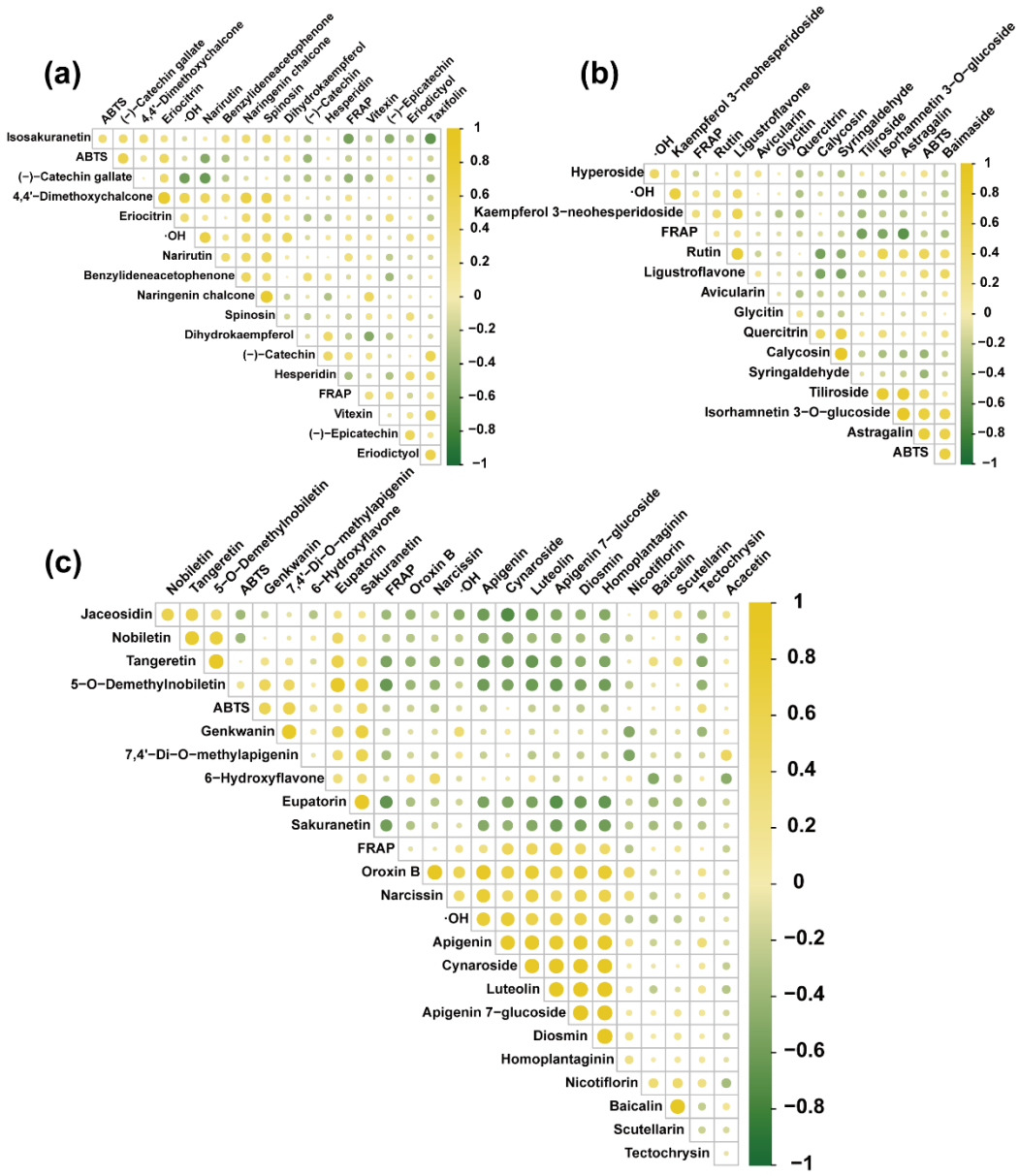

Fig. S10. Correlation of flavonoids in grains with ferric reducing antioxidant power (FRAP), 2,2'-azino-bis (3-ethylbenzothiazoline-6-sulfonic acid) (ABTs) scavenging capacity, and hydroxyl radical (•OH) scavenging capacity. (a) Correlation of chalcone, flavanols, dihydroflavone, dihydroflavonol, and flavonoid carboglycosides with FRAP, ABTs, and •OH scavenging capacity; (b) Correlation of flavonol, isoflavones, and phenolic acids with FRAP, ABTs, and •OH scavenging capacity; (c) Correlation of flavone with FRAP, ABTs, and •OH scavenging capacity.

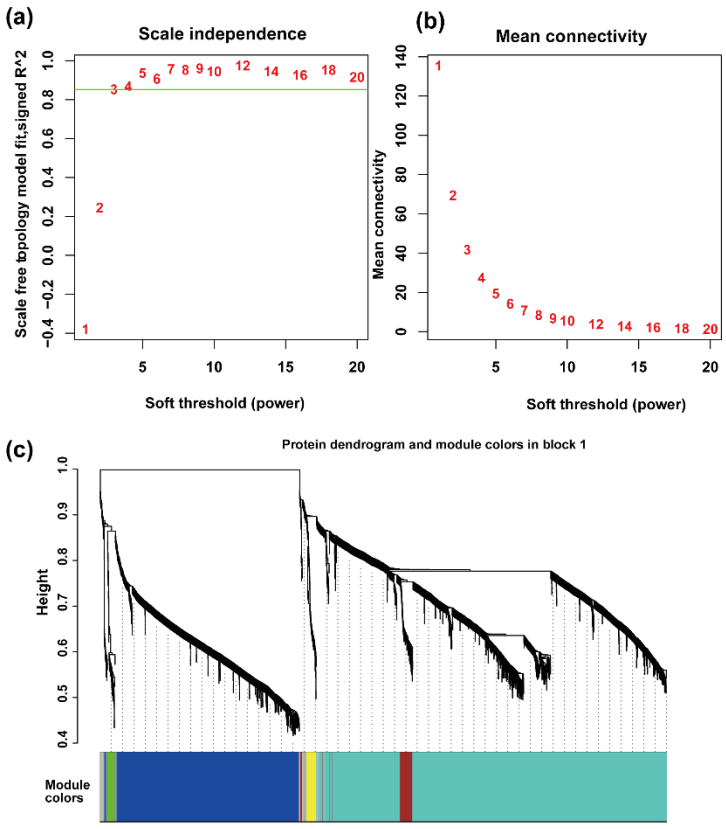

Fig. S11. Analysis of weighted gene co-expression network of rice protein under the combined pollutants of Cd-NIs. (a) Scale-free adaptive curve. The horizontal coordinate represents the power-exponential weighted β value; The vertical axis represents the degree of fit R2 between the adjacency matrix transformed from the corresponding β value and the scale-free network assumption. (b) Average connectivity curve. The horizontal coordinate represents the power-exponential weighted β value. The vertical axis represents the average connectivity (k/degree/connectivity) of each node in the network represented by the adjacency matrix after the transformation of the corresponding β value. (c) Module identification. Proteins are divided into modules based on their expression trends, where a branch represents a protein and a color represents a module. If the color is gray, it indicates a protein that has not been divided into a specific module.

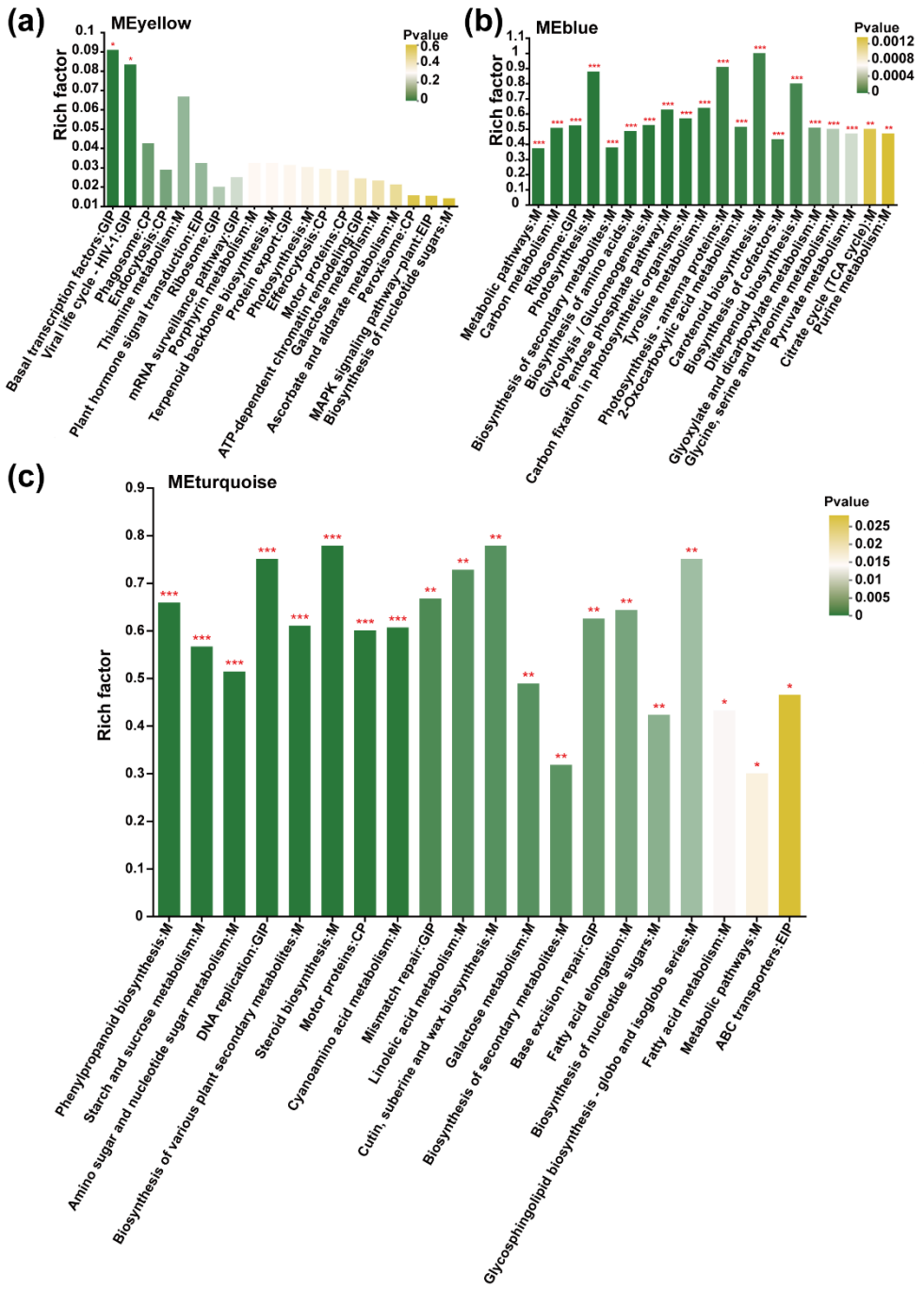

Fig. S12. The KEGG enrichment pathway of proteins in the MEyellow (a), MEblue (b), and MEturquoise module. The *p*-values are displayed on a heat map ranging from low (green) to high (yellow).

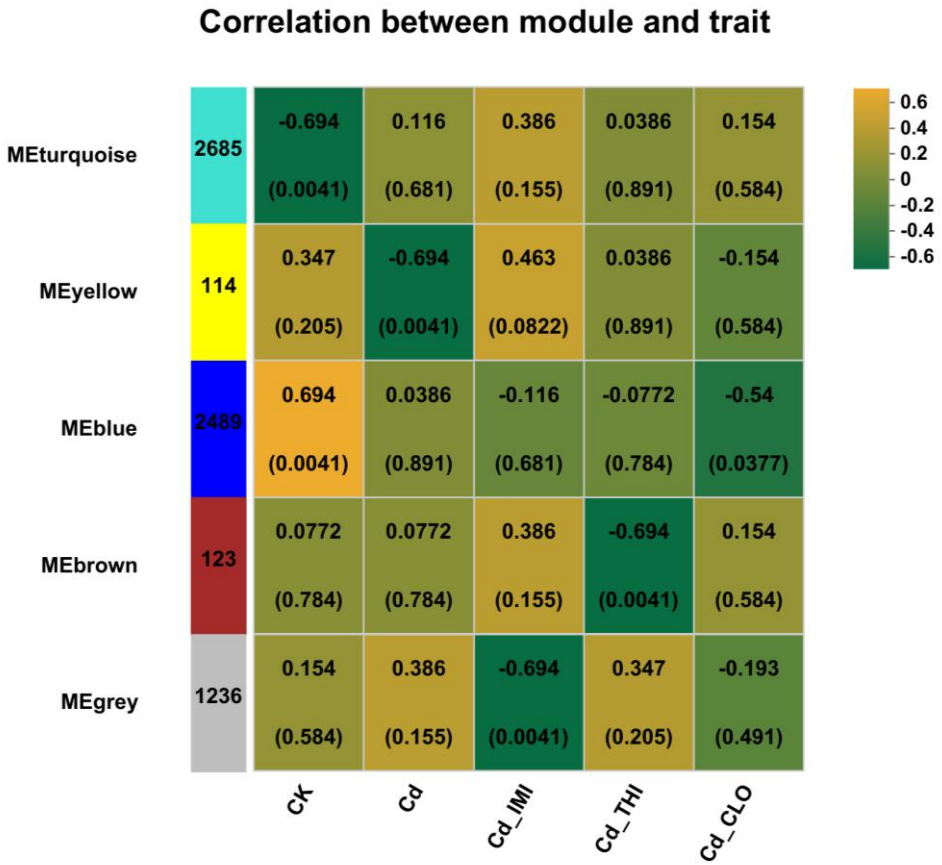

Fig. S13. Correlation analysis of modules and exposure to different pollutants in weighted gene co-expression network analysis. The correlation is shown as a heat map from low (green) to high (yellow).

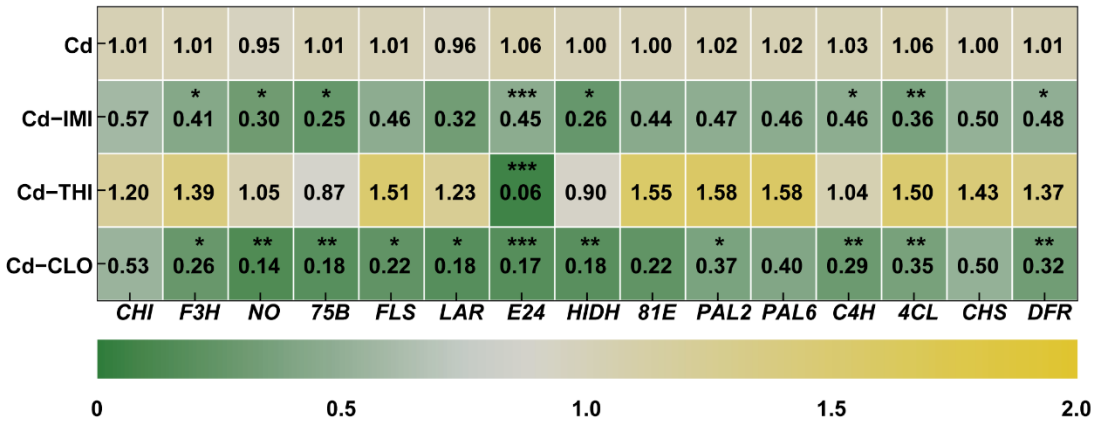

Fig. S14. Expression changes of key genes in flavonoid biosynthesis in rice leaves under the combined pollutants of Cd-NIs. Gene expression is shown as a heat map from low (green) to high (yellow). *, **, and *** indicate that the values are significantly different compared with the single Cd ($p < 0.05$, $p < 0.01$, and $p < 0.001$).

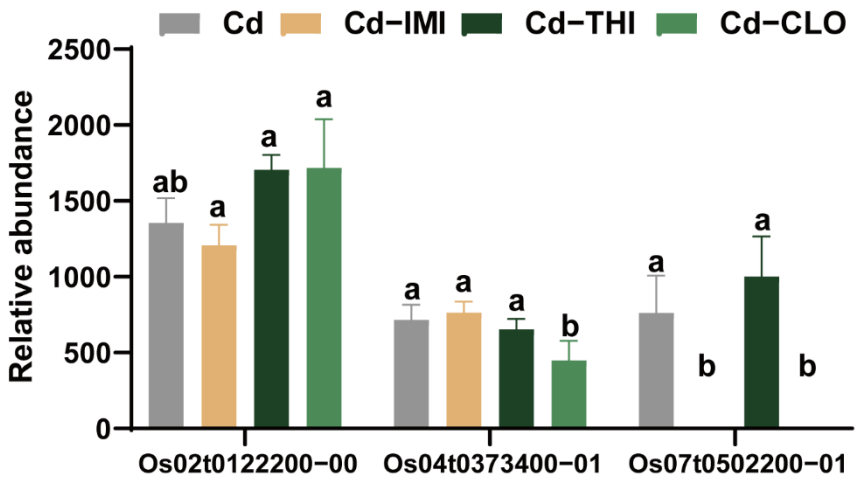

Fig. S15. The expressions of MATE transporter in the rice roots under the combined pollutants of Cd-NIs.

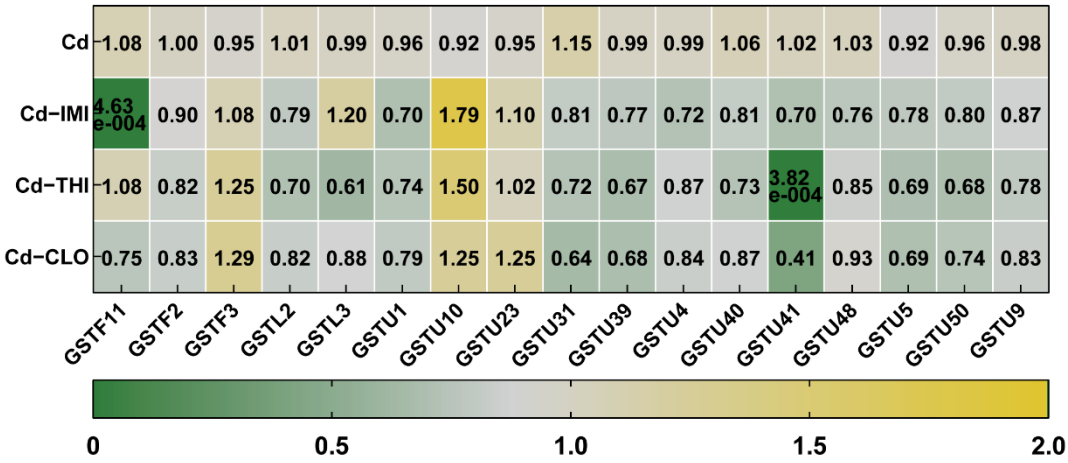

Fig. S16. The expressions of GST transferase in the rice roots under the combined pollutants of Cd-NIs.

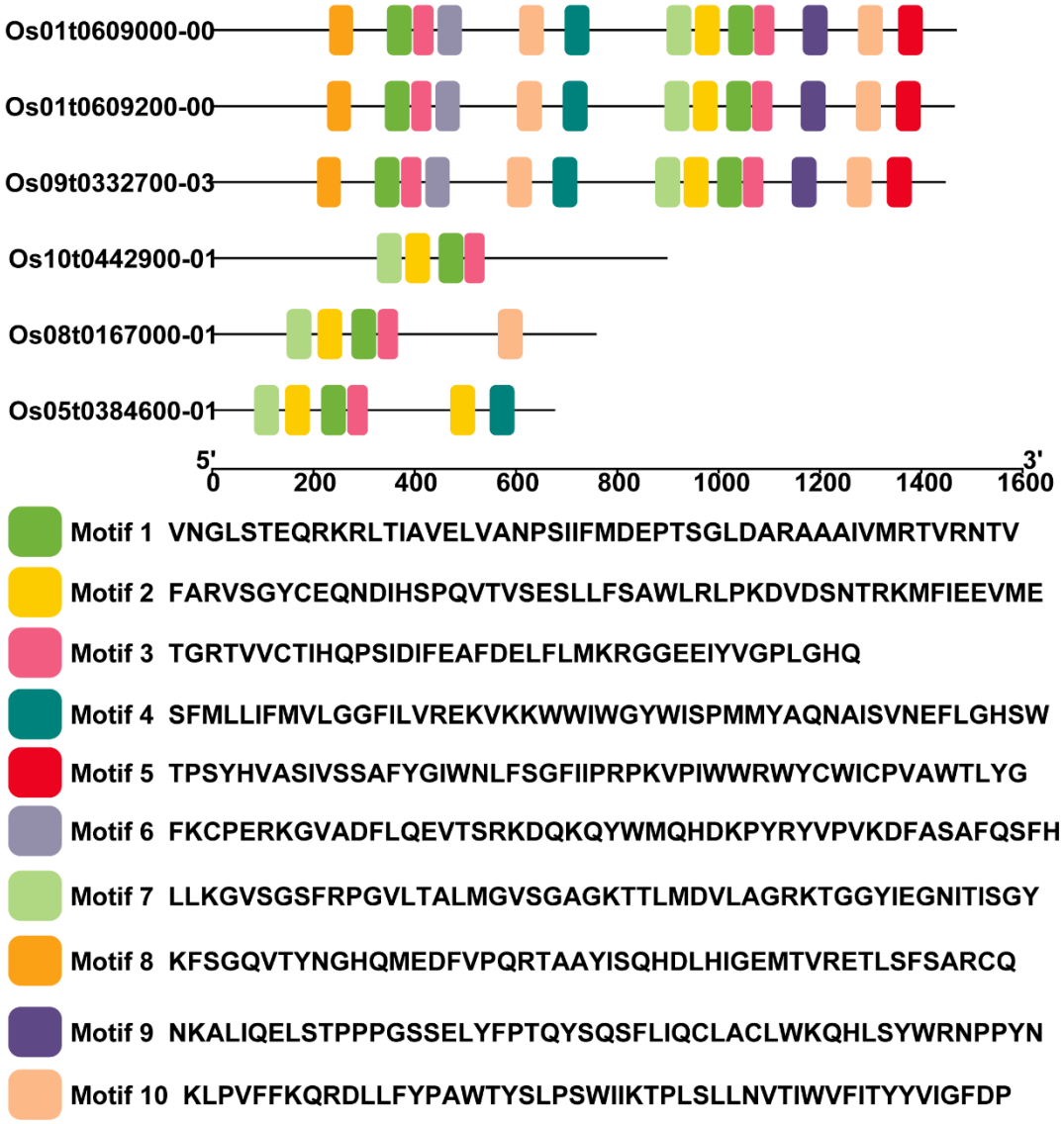

Fig. S17. Motif analysis of differential ABCG transporters.

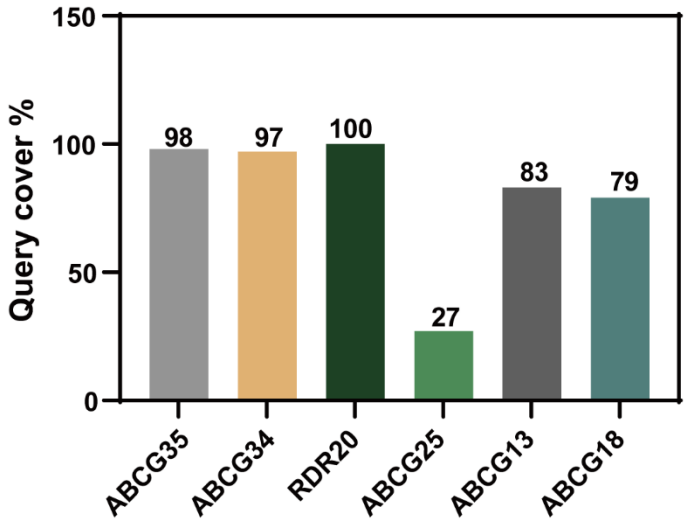

Fig. S18. Sequence alignment of differential ABCG transporter with MtABCG10 (flavonoid transporter).

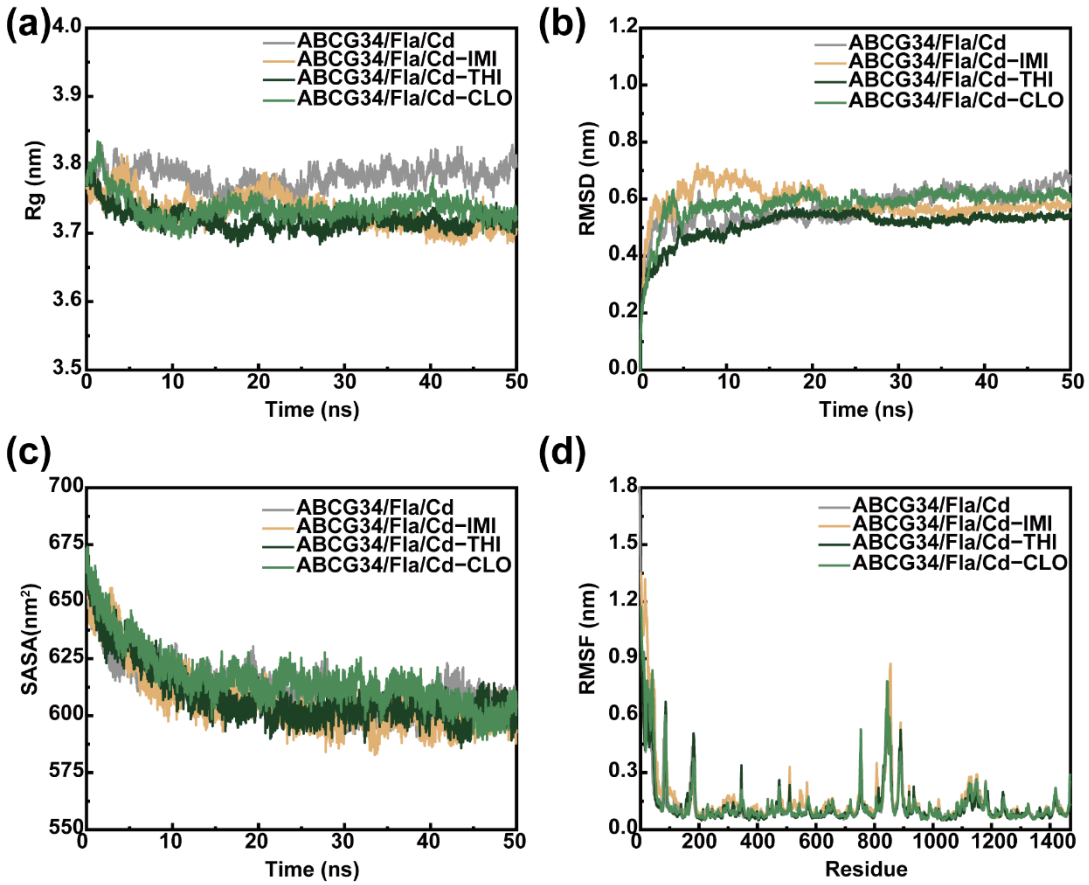

Fig. S19. The molecular dynamics (MD) simulation of the ABCG34 transporter complex with Flavonoid/Cd-NIs. Changes of radius of gyration (Rg) values (a), root mean square deviation (RMSD) values (b); solvent accessible surface area (SASA) values (c); and root mean square fluctuation (RMSF) values (d).

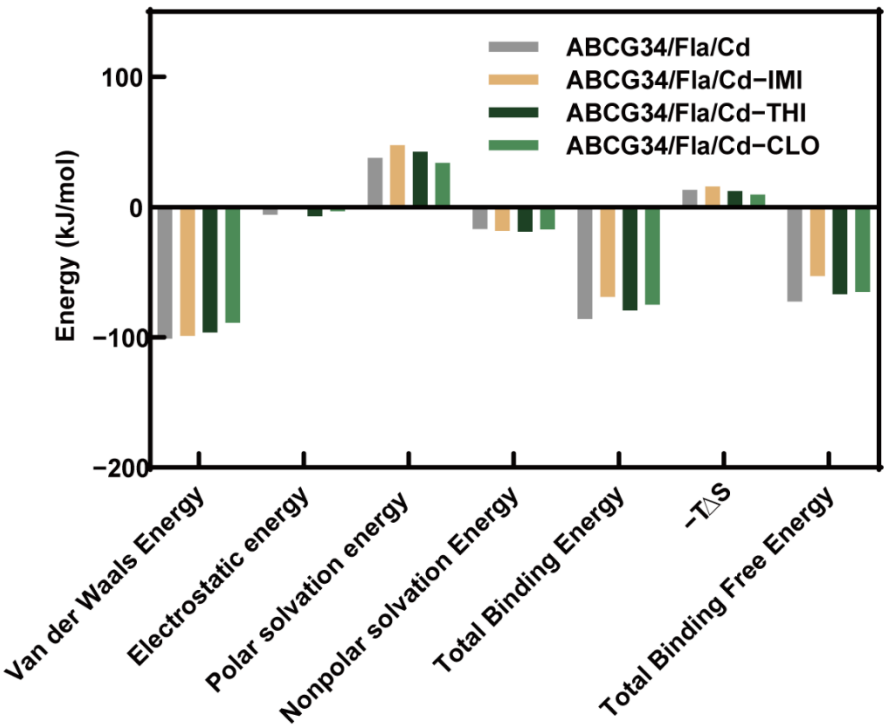

Fig. S20. Binding free energy of the abcg34 transporter complex with Flavonoid and Cd-NIs during the MD simulation.

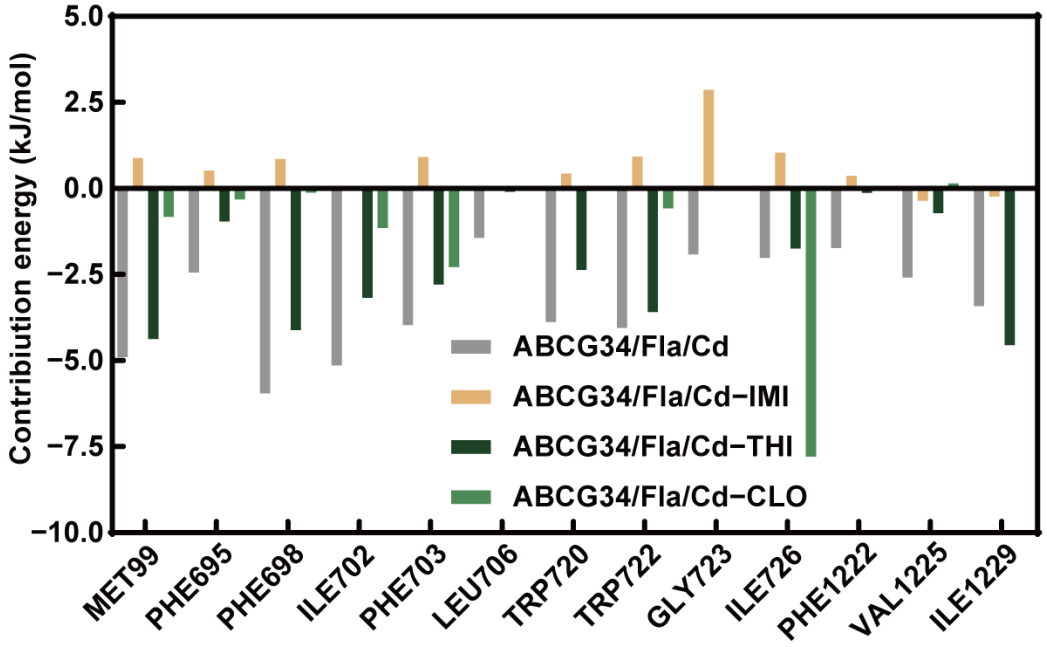

Fig. S21. Contributions to binding energy from the main residues of ABCG34 transporter interacting with Flavonoid/Cd-NIs.

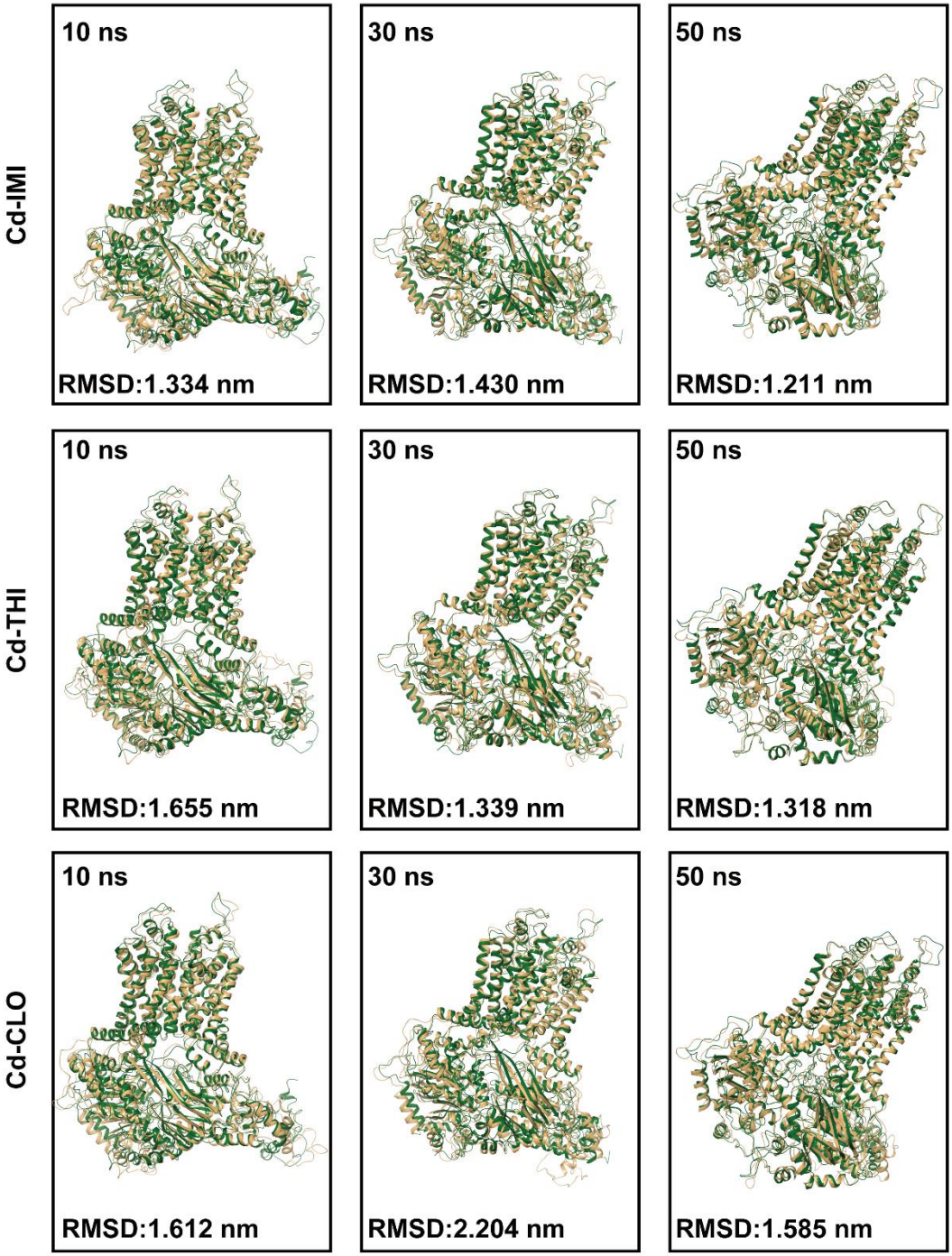

Fig. S22. Conformational changes of ABCG34 transporter during the MD simulation. The structures of 10 ns, 30 ns, and 50 ns under the Cd alone are represented with green cartoons, and the structures of 10 ns, 30 ns, and 50 ns under the combined pollutants of Cd-NIs are represented with yellow.

Tables

Table S1. The compositions of Hoagland solution

Nutrient element	Compositions	Concentration (mg/L)
N	NH_4NO_3	114.3
P	NaH_2PO_4 $2H_2O$	50.3
K	K_2SO_4	89.2
Ca	$CaCl_2$	157.0
Mg	$MgSO_4$ $7H_2O$	410
Si	Na_2SiO_3 $9H_2O$	568
Mn	$MnCl_2$ $4H_2O$	1.79
Mo	$(NH_4)_6Mo_7O_{24}$ $2H_2O$	0.09
B	H_3BO_3	1.13
Zn	$ZnSO_4$ $7H_2O$	0.04
Cu	$CuSO_4$ $5H_2O$	0.04
Fe	Fe-EDTA-Na_2 $3H_2O$	30.0

Table S2. List of real-time qRT-PCR primers for key genes in the flavonoid biosynthesis pathway

Gene name		Primer Sequences (5' → 3')
UBQ_10	Forward	TGGTCAGTAATCAGCCAGTTTGG
	Reverse	GCACCACAAATACTTGACGAACAG
PAL2	Forward	GTGTACATACACACTGCCGC
	Reverse	ACGCGCATCTGACTTGTTTG
PAL6	Forward	CTGGAGCAGGGTGTTGATGC
	Reverse	ATACTGAGAGGTTGCAAAGCTGA
C4H	Forward	ACGTCCATGCCGATTTGTCA
	Reverse	CTTCAGACGCTTCCCCTGTT
4CL	Forward	TAGATGTGGAACAGCGGCAG
	Reverse	GTGAAATTTGGTGCAGGTGGA
CHS	Forward	ACATGTTGCCGTACTCGGAC
	Reverse	GGGGATCTCGGACTGGAACT
CHI	Forward	GCGAATTAACCGCGCATCTA
	Reverse	AACAGCCGCGATTTCTCCTT
HIDH	Forward	ACCAAGTCCAAACCCTCACC
	Reverse	CGAGTTCTTCTGGGAGGCAG
FLS	Forward	GATTCGGCAGGATGGGATT
	Reverse	TTCGTGGACTCGTTGTGGC
NOMT	Forward	GCAGGGCACACTCCACATTA
	Reverse	GCATAGCCATTCCTCCCCAA
F3H	Forward	CCCCATGACACCCAAGTACC
	Reverse	GTCGGCATGGAAGGCAATTC
CYP81E9	Forward	GGCGAGAAGAAGAGCGTGAT
	Reverse	TAATGCTCACTCACCGCACA
E2.4.1.91	Forward	TTGTGCATAGCTGGAGGTGG
	Reverse	GCCGAACGACCAAAACAACC
CYP75B1	Forward	GCGCTACCCTCCTAGTCAAC
	Reverse	CGCATATTCTCCGTCCTGCT
DFR	Forward	CAACCAGACAGCAACTTGGC
	Reverse	GCTGAGGGATTTGGGGTTCA
LAR	Forward	CCACACTGCCACACTCATTG
	Reverse	CGATGGGTTCTTGCTGGCTA

Table S3. List of real-time qRT-PCR primers for genes encoding full-length ABCG transporters

Gene name		Primer Sequences (5' → 3')
UBQ_10	Forward	TGGTCAGTAATCAGCCAGTTTGG
	Reverse	GCACCACAAATACTTGACGAACAG
ABCG34	Forward	CATCTCCAGACCGGCAACTC
	Reverse	TCCACGAAGACATTCACGGG
PDR20	Forward	CCAATGTGCTGGAGGGTCTG
	Reverse	TCCAGCCAAGGCCAAAAGAA
ABCG35	Forward	CATCATCCCCAGACCGAAAGTT
	Reverse	CAAACTGCGAGGCAACCAGA